Computational Modelling of Concrete and Concrete Structures – Meschke, Pichler & Rots (Eds)

Investigation of drying shrinkage effects on sloped concrete-concrete composites

D. Daneshvar, K. Deix & A. Robisson
Research Group of Building Materials and Technology, Faculty of Civil Engineering, Vienna University of Technology (TU Wien), Vienna, Austria

Behrouz Shafei
Department of Civil, Construction, and Environmental Engineering, Iowa State University, Ames, IA, United States

ABSTRACT: Multi-layer concrete systems have been widely used in bridge decks, rigid pavements, and floors. The restrained drying shrinkage of the overlay is of great concern as it can lead to overlay cracking and/or interfacial debonding. In such constructions, a transverse slope is typically considered to drain off the surface water. Despite advances made in understanding the drying shrinkage of non-sloped concrete-concrete composites, there are still standing questions regarding the overlay cracking, as well as bond failure, in sloped concrete-concrete composites. The current study establishes a high-fidelity computational model validated with experimental tests to evaluate the structural performance of sloped, double-layer overlay systems under drying shrinkage. The simulation scenarios systematically cover the effects of key overlay properties and interface conditions. The numerical analysis results reveal the critical role of overlay thickness and mechanical properties in the time of overlay cracking and interfacial debonding failures. Based on the obtained results, the implementation of a cross slope may delay the failures, depending on the initial thickness. Higher interfacial stiffness also induces stronger restraint against overlay shrinkage strain, leading to a faster overlay cracking.

1 INTRODUCTION

Concrete overlays have been used to protect concrete structures exposed to the excessive loading and harsh environmental conditions (Emmons 1994). Not limited to repair applications, concrete overlays have also been employed in large concrete structures where several concrete pours are required at various stages of construction (Loo et al. 1995). Thus, the use of multi-layer concrete systems covers a wide range of applications such as bridge decks, rigid pavements, dams, slabs and floors. According to the American Concrete Pavement Association (ACPA), the use of concrete overlays has rapidly increased from 2% in 2000 to 12% of the entire concrete paving applications in 2017 (Gross & Harrington 2018). As a durable, cost-effective, and sustainable solution, concrete overlays provide additional strength and protect the underlying reinforced concrete layer from deleterious agents (Harrington et al., 2007). Therefore, it is essential for the overlays to retain their strength under a wide variety of mechanical and environmental stressors (Çolak et al. 2009; Daneshvar et al. 2021; Emmons 1994).

Drying shrinkage represents a major issue upon constructing overlays. In multi-layer concrete systems, the water loss from the overlay is attributed to the environmental drying, ongoing hydration, and moisture absorption by the concrete substrate. As the drying shrinkage-induced strains of the concrete overlay are restrained by the concrete substrate, they cause tensile stresses in the overlay, and additional shear (friction) and normal (delamination) stresses at the interface of the overlay and the concrete substrate (Li & Li 2006). These induced stresses are influenced by the magnitude of overlay's shrinkage such that larger shrinkage of the overlay results in higher stresses and hence a higher risk of failure. Overlay cracking and/or interface debonding are the most common types of failures observed in concrete-concrete composites (Emmons & Vaysburd 1994). The outlined failure modes impact the load transfer mechanism between concrete layers, causing a non-monolithic behavior that eventually jeopardizes the load-bearing capacity and overall structural performance of the concrete-concrete composites. Such defects can also facilitate the ingress of water and deleterious agents into the composite system, resulting in long-term durability issues and extensive repair needs.

Moreover, during the lifetime of concrete overlays, standing surface water is a major concern. Ponding of water on the overlay surface can result in slippage, hydroplaning, and icing in winter, while facilitating the gravitational ingress of standing water into the reinforced concrete substrate (Smith et al. 2014). A

DOI 10.1201/9781003316404-75

sufficient transverse slope, however, can ensure the proper drainage of surface water from the overlay and minimize its associate issues. To drain off the surface water, a transverse cross slope is typically considered for the overlay. The American Association of State Highway and Transportation Officials (AASHTO) policy on geometric design of highways and streets recommends a cross slope of 2% for usual conditions to mitigate the risk of hydroplaning. Depending on the rainfall and application, a lower or higher cross slope can also be implemented (AASHTO 2011).

Previous studies investigated the effects of overlay properties, interface conditions, external environmental conditions, and boundary conditions on the structural performance and durability of concrete-concrete composites subjected to drying shrinkage (Li & Li 2006; Santos & Julio 2011). Despite advances made in understanding the drying shrinkage of non-sloped concrete-concrete composites, there are still standing questions regarding the crack formation, as well as bond failure, in sloped concrete-concrete composites. Furthermore, numerous shrinkage and creep prediction models have been developed based on extensive experimental datasets. Although these models have been widely and successfully used, most of the finite-element (FE)-based studies used an analytical or semi-analytical approach to take shrinkage and creep behavior of concrete into consideration. These approaches, in most cases, employed a heat transfer analysis, missing factors contributing to shrinkage and creep.

Given the outlined research gaps and questions, the current study established a high-fidelity computational model validated with experimental tests to evaluate sloped, double-layer concrete systems under drying shrinkage. For this purpose, three-dimensional FE simulations were performed. The shrinkage strain and creep coefficient of concrete were incorporated as a function of time based on the criteria of the empirical American Concrete Institute model (ACI 209.2R-08 2008). The simulation scenarios under consideration systematically cover the effects of key overlay properties and interface conditions, such as overlay geometry (thickness and slope), overlay material properties, and interfacial degree of restraint. The outcome sheds light on the optimized combinations of overlay geometries and interfacial conditions required to enhance the short- and long-term performance of concrete-concrete composites.

2 MODELLING AND VALIDATION

2.1 *Numerical model*

The Abaqus software package (2021) was used in this study. The concrete overlay was modeled with a length of 5 m and a width of 2 m. The overlay length was selected long enough (greater than 2 times of the width) to account for the continuity of the overlay. The thickness and slope of the overlay were varied between 20 and 200 mm, and 0 and 10% slope, respectively. The overlay crowned surface slopes from both sides of the centerline. The substrate length was 8 m with a width of 4 m and a constant thickness of 200 mm. Due to the symmetry of the models, a quarter of the described concrete-concrete composites were modeled. Figure 1 shows the generated 3D FE model.

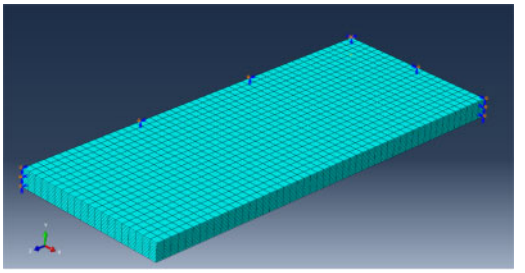

Figure 1. 3D FE model generated for numerical simulations.

As for boundary conditions, the bottom surface of the substrate was fixed against translation in all three orthogonal directions. Due to the restraint provided by adjacent layers, the movement of the lateral faces of the substrate were fixed via a roller support. 20-node quadratic brick elements (C3D20) were used for the model. Considering the mesh sensitivity analysis and cracking occurrence in the overlay, a finer mesh was employed for the overlay while the substrate was modeled with a coarser mesh. The interface between concrete layers was modeled by including a cohesive contact behavior. This contact allows to capture possible delamination at the interface. The bi-linear separation-traction and force-slip constitutive curves were employed to formulate the cohesive contact behavior. They are typically characterized by penalty stiffness defined as the slope of linear elastic part (pre-damage response) and peak strength (damage initiation). The normal and shear bond strength was assumed as 1.5 and 3.0 MPa, respectively, according to the experimental values reported in the literature (Momayez et al. 2005). Depending on the degree of restraint between concrete layers, a wide range of interfacial normal and shear stiffnesses is proposed (Tsioulou & Dritsos 2011). To account for this, and based on the experimental results reported in the literature, the interfacial stiffness between concrete layers was modeled with values in the range of 0.5 to 100 N/mm^3. The concrete damage plasticity model (CDP) was utilized to represent the behavior of the concrete layer in both elastic and plastic domains. Depending on the application and field requirements, various types of overlays have been utilized, among which the normal-strength concrete (NC) and ultra high-performance concrete (UHPC) are the most common types (Gross & Harrington 2018; Haber et al. 2017). Therefore, to compare their structural performance, these two concrete types (i.e., NC and UHPC) were considered for the overlay while the substrate was modeled with NC. For this purpose, experimental tests including uniaxial tensile, compressive and elastic modulus tests

were carried out to capture their behavior at 28 days. Table 1 presents the experimental results used for the properties of concrete overlay and substrate in the simulations.

Table 1. Experimental results of concrete properties at 28 days.

Properties	Value	
	NC	UHPC
Tensile strength (MPa)	3.6	8.3
Compressive strength (MPa)	63.4	134.3
Elastic modulus (GPa)	26.3	36.2
Density (kg/m^3)	2400	2500
Poisson's ratio	0.2	0.2

2.2 *Drying shrinkage simulation*

The empirical ACI 209 shrinkage and creep model was employed to simulate the shrinkage strain and creep of concrete as a function of time (ACI 209.2R-08 2008). Thermal loading was artificially used to input shrinkage and creep. For this purpose, the UEXPAN and USDFLD user subroutines were developed. The UEXPAN subroutine applied a thermal strain increment, which represented the defined time-dependent strain caused by the shrinkage and creep of concrete. The USDFLD subroutine stored the elastic strains in each increment as state variables, which were used in creep strain calculations. In ACI 209, the time-dependent shrinkage and creep strain are described based on the age of the concrete, curing method, time of drying, relative humidity, volume to surface ratio, slump, fine aggregate to total aggregate ratio, cement content, and air content (ACI 209.2R-08 2008). Table 2 lists the coefficients and correction factors used in the FE simulations. The age of concrete at the start of drying and loading was set to 2 days. In this study, the development of drying shrinkage was considered during the first three months of casting so that the time period of analysis was set at 9×10^6 seconds (104 days).

Table 2. Correction factors for shrinkage strain and creep coefficient based on ACI 209 model.

Correction factor	Value	
	Shrinkage	Creep
Initial moist curing	1.13	–
Age of loading	–	1.15
Ambient relative humidity	0.69	0.8
Member size factor	0.33	0.67
Slump factor	1.03	1.05
Fine aggregate factor	1	1
Cement content factor	0.97	1
Air content factor	0.99	6
Time ratio (α, ψ)	0.85	0.6
Time ratio (f, d)	35	15
Ultimate shrinkage strain	1.3	–
Ultimate tensile creep	–	1.8
Ultimate compressive creep	–	1.4

2.3 *Validation*

To validate the developed FE models, the structural performance of a concrete-concrete composite model was compared to the experimental results reported by (Li & Li 2006). Similar material properties, geometry and boundary conditions were employed in the model. Figure 2 compares the end corner delamination height of the overlay in the model with the data measured experimentally. As can be seen, the results extracted from the FE simulation are consistent with those experimental measurements. Specifically, a similar evolution of delamination height tends to prove consistent drying shrinkage strain and stress distribution in both cases. Moreover, the overlay cracking occurred within the first 7 days in both cases. It must be pointed out that the Abaqus standard solver was used to capture the failure occurrence and its corresponding time in each simulation. Therefore, the numerical analysis continued only until cracking occurrence. Thus, large plastic deformations are not part of this study.

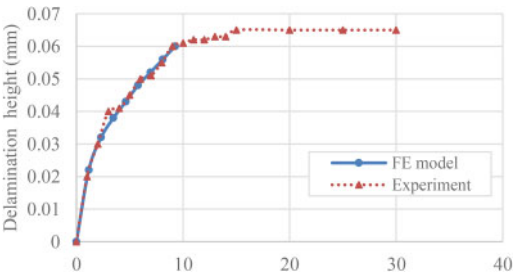

Figure 2. Comparison of the FE model results with the experimental test data recorded for the corner delamination height in concrete-concrete composites over time.

3 NUMERICAL ANALYSIS AND RESULTS

Overlay cracking and interface debonding make up a majority of failures in concrete-concrete composites. Therefore, the emphasis of this study is on evaluating the occurrence of these two types of failure, as a function of overlay geometry (thickness and slope), overlay material properties, and interfacial degree of restraint (normal and shear stiffness). Specifically, the onset of the development of maximum principal plastic strain, based on the CDP model, was considered as the overlay cracking occurrence. To determine the interfacial failure, based on the defined bi-linear traction-separation behavior, the corresponding time to the state in which the separation and/or slip between layers exceeds the maximum allowable strength (damage initiation) was taken as the interfacial debonding/slippage failure. Before damage initiation, the behavior of the cohesive contact is ensured. This was defined as a linear elastic behavior so the interfacial debonding and slippage thresholds are calculated by dividing the defined bond strength to the corresponding interfacial

stiffness. It must be highlighted that debonding was the only type of interfacial failure that occurred in the models that experienced failure. Figure 3 show the typical 3D stress distribution and deformed shaped of the concrete overlay subjected to the restrained drying shrinkage.

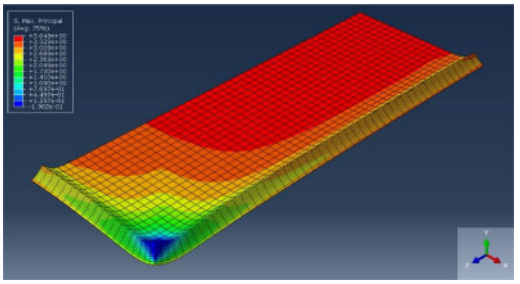

Figure 3. Typical 3D deformed shape of the overlay in the FE model subjected to restrained drying shrinkage. The contours represent the maximal principal stress before damage initiation. Deformations are amplified by a factor of 3000 for visualization purposes.

3.1 *Thickness*

The concrete overlay thickness varies depending on the purpose of the application, overlay material properties, and field limitations. Thus, based on the reported values in the literature, a broad range of thicknesses, between 20 and 200 mm, was considered in this study. Figure 4 shows the overlay cracking and interfacial debonding corresponding times. To capture the effect of thickness on concrete-concrete composites failure, the thresholds for cracking of NC overlay and debonding of the interface were set at 3.6 MPa and 0.03 mm, respectively. As can be seen, increasing the overlay thickness from 20 mm to 100 mm leads to a negligible increase (2 days) in overlay cracking time. However, further increasing the thickness results in a drop of overlay cracking time by 10 days. Moreover, the interface debonding occurred earlier than overlay cracking in composites containing thick overlays (above 100 mm).

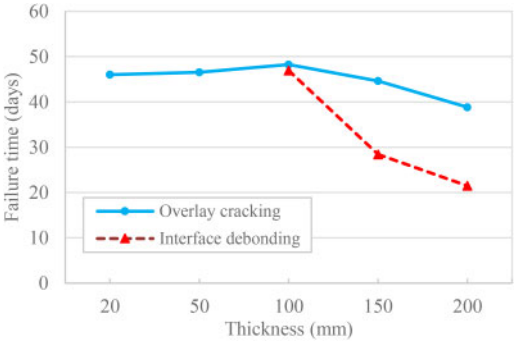

Figure 4. Overlay drying shrinkage cracking and interface debonding corresponding times as a function of overlay thickness.

The drying shrinkage cracking in overlays with a thickness up to 100 mm was initiated from the center part of the overlays where the induced tensile stress was highest. However, further increasing the thickness resulted in the shift of cracking location to the end corners of the overlay. To compare the stress evolution in overlays with different thicknesses, the stresses induced by the restrained drying shrinkage are plotted in Figure 5 and Figure 6. It must be highlighted that the results are plotted at time of 1.75 × 106 seconds (20 days). This time was the latest possible time at which all the composites were still intact (without any overlay cracking and interface debonding) so that the development of the stresses was not influenced by any stress release through failure occurrence. As shown in Figure 5 and Figure 6, the interfacial shear and normal stresses are predominant at the outer edge and gradually increase in thicker overlays. This is mainly attributed to the significantly higher differential displacement between the top free surface and the bottom restrained surface in thicker overlays. Specifically, this was found to increase from 0.004 to 0.042 mm upon increasing the overlay thickness from 20 to 200 mm. In case of having interfacial restraint, the higher tendency of the overlay to move, the greater the induced interfacial normal and shear stresses. In thick overlays,

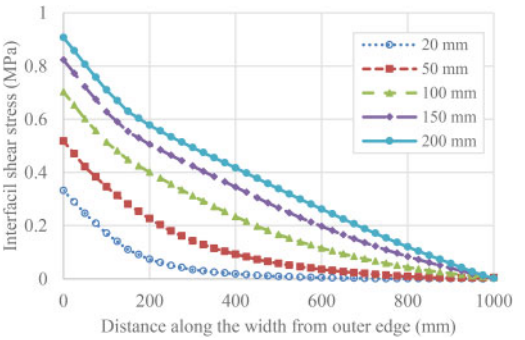

Figure 5. Distribution of interfacial shear stress along the width of concrete overlays with thicknesses from 20 to 200 mm.

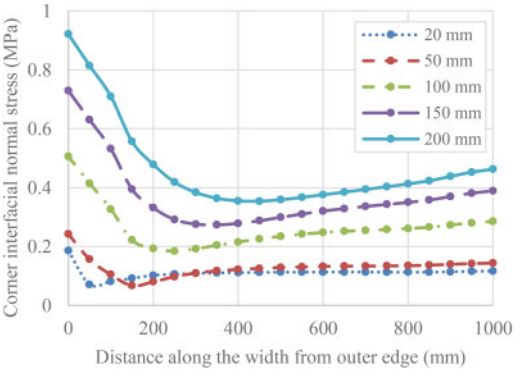

Figure 6. Distribution of corner interfacial normal stress along the width of concrete overlays with thicknesses from 20 to 200 mm.

the interfacial normal stresses in end corners exceeded the thresholds earlier than the center part, resulting in a faster occurrence of debonding and development of plastic strains. On the other hand, in thin overlays where the differential shrinkage deformation between the bottom and the top overlay surfaces was not remarkable, the induced tensile stress was concentrated in the center part of the overlay, and therefore, surface cracking was the predominant type of failure.

3.2 *Slope*

To evaluate the effect of slope in various applications, the overlay cross slope up to 10% was considered with crowned surfaces such that the overlay surface slopes from either side of the centerline. Figure 7 compares the corresponding overlay cracking times. In thin overlays (20 and 50 mm in the outer side, i.e., thinnest part), implementation of a cross slope up to 5% provides better resistance against induced tensile stress and hence extends the overlay cracking time. However, employing a cross slope of 10% in thin overlays and all cross slopes in thick overlays (100 and 150 mm) results in a faster overlay cracking. Furthermore, in each specific cross slope, increasing the thickness from 20 to 50 mm leads to an increase in overlay cracking time. It must be pointed out that overlay cracking location was observed at the end corners in case of thick sloped overlays. These results are consistent with the effect of thickness described in the previous section, i.e., increasing the cross slope leads to a transverse increase in the overlay thickness and intensifies end corner delamination.

Interfacial debonding occurred prior to the overlay cracking in thick overlays (100 and 150 mm) including all implemented slopes. For thinner overlay, the interface failure was never observed within the studied time.

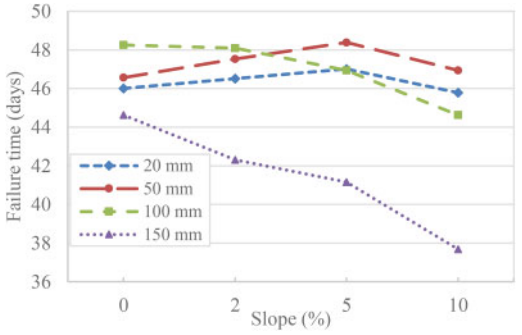

Figure 7. Overlay drying shrinkage cracking times as a function of overlay cross slope and thickness.

3.3 *Interfacial stiffness*

The non-sloped overlay with a thickness of 100 mm was used in this set of simulations. Greater interfacial stiffness typically induces stronger restraint against overlay displacement along the interface, inducing higher shear and tensile stress. This led to an overlay cracking in composites with an interfacial stiffness greater than 1 N/mm^3 (Figure 8). Specifically, there is a sharp drop of 30 days in overlay cracking time upon increasing the interfacial stiffness from 2 to 20 N/mm^3. In composites with a smoother interface and lower interfacial stiffness (0.5 and 1 N/mm^3), the drying shrinkage of the overlay is less restrained and hence the induced tensile and shear stress stayed below the overlay strength, and thus, cracking was not observed within the studied time period (104 days).

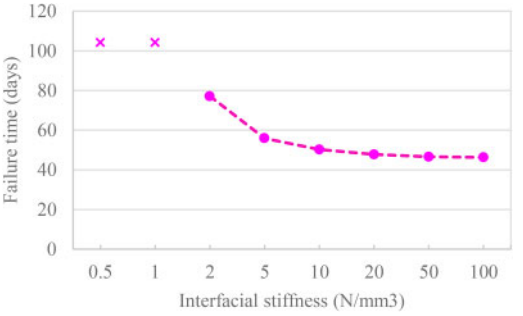

Figure 8. Overlay drying shrinkage cracking times as a function of interfacial stiffness. The cross marks represent points where failure did not occur during analysis time period.

3.4 *Overlay strength*

The effect of overlay characteristics was assessed by comparing the structural performance of UHPC with conventional NC. The non-sloped overlay with a thickness of 100 mm was used in the simulation. Figure 9 compares the structural performance of normal and UHPC overlays in concrete-concrete composites subjected to the restrained drying shrinkage. In all the studied cases, the UHPC resisted the induced tensile and shear stress, and hence the drying shrinkage cracking did not occur within the studied period time (104 days). This is mainly due to the superior mechanical properties of UHPC and specifically its high tensile strength, which was 2.3 times greater than that of NC. It must be highlighted that the main part of induced stress was released thorough end corner interface

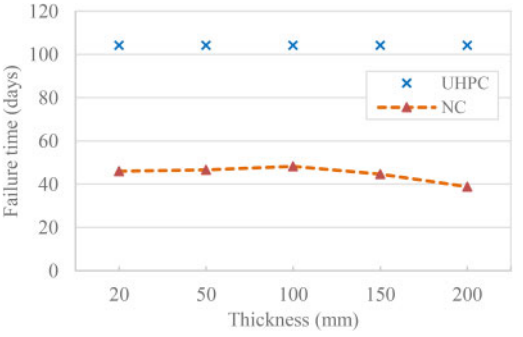

Figure 9. Comparison of NC and UHPC overlay drying shrink-age cracking times. The cross marks represent points where failure did not occur during the analysis time period.

delamination. Increasing the overlay thickness intensified this phenomenon and resulted in early-stage interfacial debonding failure.

Figure 10 shows the interfacial performance of composites including UHPC and NC overlay. As described before, the greater resistance of UHPC against induced tensile and shear stresses leads to the predominant mechanism of stress release through end corner interface delamination. Therefore, the debonding failure occurs (3–10 days) earlier in UHPC overlaid composites than NC ones.

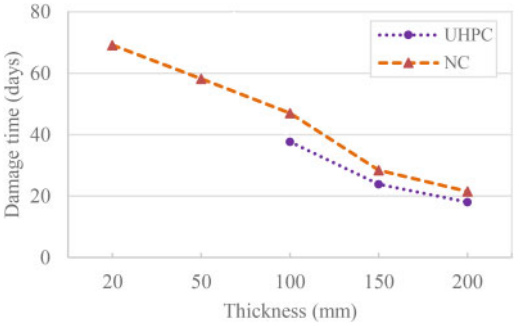

Figure 10. Comparison of NC and UHPC overlay drying shrinkage cracking times. The cross marks represent points where failure did not occur during the analysis time period.

4 CONCLUSIONS

The effects of overlay geometry (thickness and slope), overlay material properties, and interface restraint conditions were investigated in concrete-concrete composites subjected to drying shrinkage. The numerical analysis results showed that the overlay thickness plays a pivotal role in the structural performance of the composites. It was found that there is an optimum point for the overlay thickness (in this study, 100 mm), below which the overlays are more vulnerable to restrained shrinkage and demonstrate earlier cracking. Employing thicker overlays, on the other hand, was found to result in a significant end corner delamination and hence early-stage interfacial debonding. Consistent with this, the effect of overlay transverse slope was determined to depend on the initial thickness of the overlay such that for the overlays up to 50 mm thick, the overlay crack can be delayed by employing a cross slope up to 5%.

Further increasing the cross slope and employing higher initial thickness would adversely impact the structural performance of concrete-concrete composites through early-age overlay cracking and/or interfacial debonding. Furthermore, the interfacial degree of restraint was found to significantly affect the performance of the double-layer concrete systems such that a sharp drop of 30 days in overlay cracking time was observed upon increasing the interfacial stiffness from 2 to 20 N/mm^3. In the case of smoother interfaces, i.e., with an interfacial stiffness less than 2 N/mm^3, the overlay restrained shrinkage strain was insignificant to the extent that overlay drying shrinkage cracking did not occur. The type and mechanical properties of the overlay materials also influenced the behavior of the concrete-concrete composites under restrained drying shrinkage conditions. It was found that application of UHPC overlay can delay the overlay shrinkage cracking at least 60 days compared to the NC overlays. However, the end corner interface delamination occurred earlier in UHPC overlays.

REFERENCES

ACI 209.2R-08. (2008). *Guide for Modeling and Calculating Shrinkage and Creep in Hardened Concrete*. American Concrete Institute, USA.

American Association of State Highway and Transportation Officials. (2011). *A Policy on Geometric Design of Highways and Streets*. Washington, DC, USA.

Çolak, A., Çoşgun, T., & Bakirci, A. E. (2009). Effects of environmental factors on the adhesion and durability characteristics of epoxy-bonded concrete prisms. *Construction and Building Materials*, *23*(2), 758–767. https://doi.org/10.1016/j.conbuildmat.2008.02.013

Daneshvar, D., Deix, K., & Robisson, A. (2021). Effect of casting and curing temperature on the interfacial bond strength of epoxy bonded concretes. *Construction and Building Materials*, *307*, 124328. https://doi.org/10.1016/j.conbuildmat.2021.124328

Emmons, P. H., & Vaysburd, A. M. (1994). Factors affecting the durability of concrete repair: the contractor's viewpoint. *Construction and Building Materials*, *8*(1), 5–16. https://doi.org/10.1016/0950-0618(94)90003-5

Emmons, Peter H. (1994). *Concrete Repair and Maintenance Illustrated*. R. S. Means Company.

Gross, J., & Harrington, D. (2018). *Guide for the Development of Concrete Overlay Construction Documents* (Issue August).

Haber, Z. B., Munoz, J. F., & Graybeal, B. A. (2017). *Field Testing of an Ultra-High Performance Concrete Overlay*. https://www.fhwa.dot.gov/publications/research/infrastructure/structures/bridge/17096/index.cfm

Harrington, D., DeGraaf, D., Riley, R., Rasmussen, R. O., Grove, J., & Mack, J. (2007). *Guide to Concrete Overlay Solutions* (Issue January).

Li, M., & Li, V. C. (2006). Behavior of ECC-concrete layered repair system under drying shrinkage conditions. In *Restoration of Buildings and Monuments* (pp. 143–160).

Loo, Y. H., Peterson, J. S., Swaddiwudhipong, S., & Tam, C. T. (1995). Application of the layering method on large concrete pours. *Magazine of Concrete Research*, *47*(172), 209–217. https://doi.org/10.1680/macr.1995.47.172.209

Momayez, A., Ehsani, M. R., Ramezanianpour, A. A., & Rajaie, H. (2005). Comparison of methods for evaluating bond strength between concrete substrate and repair materials. *Cement and Concrete Research*, *35*(4), 748–757. https://doi.org/10.1016/j.cemconres.2004.05.027

Santos, P. M. D., & Julio, E. N. B. S. (2011). Factors affecting bond between new and old concrete. *ACI Materials Journal*, *108*(4), 449–456. https://doi.org/10.14359/51683118

Smith, K., Harrington, D., Pierce, L., Ram, P., & Smith, K. (2014). *Concrete Pavement Preservation Guide, Second Edition* (Vol. 32, Issue 5).

Tsioulou, O. T., & Dritsos, S. E. (2011). A theoretical model to predict interface slip due to bending. *Materials and Structures/Materiaux et Constructions*, *44*(4), 825–843. https://doi.org/10.1617/s11527-010-9669-6